INSTITUTE OF PHYSICS PUBLISHING JOURNAL OF PHYSICS D: APPLIED PHYSICS

J. Phys. D: Appl. Phys. **38** (2005) 1599–1607 doi:10.1088/0022-3727/38/10/015

Experimentally fitting the attraction strength of an interface by the response of the thickness shear-mode acoustic wave sensor

F Lu[1], H P Lee[1,2], P Lu[1], X D Su[3] and S P Lim[2]

[1] Institute of High Performance Computing, 1 Science Park Road, #01-01 The Capricorn, Singapore Science Park II, Singapore 117528, Singapore
[2] Department of Mechanical Engineering, National University of Singapore, 9 Engineering Drive 1, Singapore 117576, Singapore
[3] Institute of Materials Research Engineering, 3 Research Link, Singapore 117602, Singapore

Received 6 January 2005, in final form 15 March 2005
Published 6 May 2005
Online at stacks.iop.org/JPhysD/38/1599

Abstract
The thickness shear-mode (TSM) sensor is extended for operating in a liquid environment for application in biological engineering. The interfacial effect between the sensor surface and the attached medium is one of the major controversies in modelling of the TSM resonator in a liquid environment. Several slip models have been proposed to describe the interfacial mechanism of a TSM resonator in a liquid environment. In this paper, the correlation between the spring–damper model and other slip models is presented. Three TSM sensors with different surface modifications were fabricated to verify the models. The results of the measured experimental frequency shifts are found to deviate from theoretical results evaluated using a non-slip model. By adjusting the attraction strength between the contacted interfaces, the results can be fitted by the spring–damping interface model.

1. Introduction

Acoustic wave devices are used in a sensitive technique in chemical and biological sensing [1, 2]. An AT-cut quartz thickness shear-mode (TSM) resonator is the most common structure used in this area. A typical TSM resonator consists of a thin disc of AT-cut quartz crystal with two metal electrodes deposited on both sides. Due to the piezoelectric properties and crystalline orientation of the quartz, the application of a voltage on the electrodes induces a thickness shear deformation within the crystal. The oscillating voltage applied on the electrodes generates a shear wave within the crystal resonator. The Sauerbrey equation gives the linear relationship between the resonance frequency and the surface mass density of the layer attached on the sensor surface [3]. When the TSM sensor is operated in a liquid environment, the thickness shear wave propagates into the liquid, and the liquid properties can be characterized by measuring the resonance frequency and the dissipation factor of the device [4]. The non-slip condition, normally assumed at the solid–liquid interface, leads to the continuous boundary conditions for resolution of the set of differential equations [5, 6]. Recent research showed that there is significant deviation of the frequency shift between measured and evaluated results for a TSM sensor operating in a liquid environment [7, 8]. Due to the rapid motion of the particles on the sensor surface, which is in contact with the liquid medium, there is complex hydrodynamic behaviour at the solid–liquid interface. The interfacial coupling properties play an important role in the measurement precision of the TSM sensor. The contact region at the interface experiences a high shear vibration rate which may result in strong slip between the solid and liquid contact layers.

Several interface models have been proposed to describe the slip at the solid–liquid interface. Ferrante *et al* [9] proposed a complex value of the slip parameter, which is defined as the ratio between the displacements of the contact interfaces, to describe the slip condition. McHale *et al* [10] used a single real value of the friction coefficient in electrical equivalent models for TSM resonators in liquids. Ellis *et al* [11–13] proposed a framework for a predictive model of the interface slip based

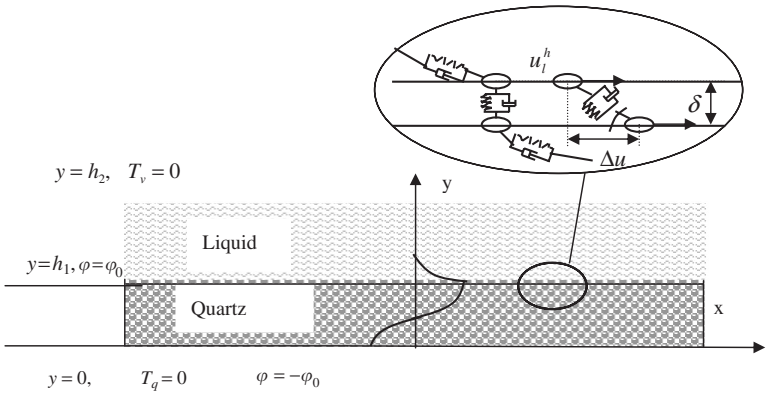

Figure 1. Slip interface model of the TSM sensor in a viscoelastic liquid environment with six boundary conditions.

on the surface–liquid slip length. In an early paper [14], a spring–damping model at the solid–liquid interface has been proposed to analyse the TSM resonator performance in a liquid. The continuous displacement and stress boundary conditions are replaced by the equations of motion of the molecular contact layers. The attraction strength, the bulk liquid viscosity and the contact molecule size are included in the model. The parameters of these models are interchangeable. In this paper, several interface slip models proposed to describe the TSM sensor in the liquid are reviewed and the correlation between these models is discussed first. Three types of TSM sensor with different surface monolayer modifications are used to verify the slip phenomenon. The experimental frequency shift measured can be matched by adjusting the real portion of the attraction strength in the slip modelling.

2. Theoretical treatment of TSM resonators in liquid with interfacial slip

TSM devices can be described by a set of differential equations, including the piezoelectricity, elastic equation and fluid equation. Due to the high ratio between the width and thickness of a quartz plate, the effect of the lateral dimension may be reasonably ignored and the problem is simplified into a one-dimensional problem. Only the thickness shear vibration mode is generated within the quartz plate, which propagates in the thickness direction. A set of differential equations based on linear piezoelectricity, Newton's law and the Navier–Stokes equation are required to solve the problem [9]. Considering a travelling wave generated with frequency ω, the harmonic solution of the shear displacement profile within the quartz plate and in the liquid can be written as the sum of the travelling waves in the positive and in the negative directions by [15]

$$u_q = (A_1 \mathrm{e}^{-\mathrm{j}k_q y} + B_1 \mathrm{e}^{\mathrm{j}k_q y})\mathrm{e}^{\mathrm{j}\omega t}, \tag{1}$$

$$u_v = (A_2 \mathrm{e}^{-\mathrm{j}k_v y} + B_2 \mathrm{e}^{\mathrm{j}k_v y})\mathrm{e}^{\mathrm{j}\omega t}, \tag{2}$$

where $k_q = \omega\sqrt{\rho_q/\hat{c}_q}$, $k_v = \omega\sqrt{\rho_v/\hat{c}_v}$ are the complex wave numbers of the quartz crystal and the liquid, respectively, ρ_q, ρ_v being the density of quartz and the liquid; $\hat{c}_q = c_{66}^q + \mathrm{j}\omega\eta_q + e_{26}^2/\in_{22}$ is the piezoelectric stiffness modulus, c_{66}^q being the quartz shear modulus, η_q the quartz viscosity, e_{26} the piezoelectric constant and $\in_{22}$ the dielectric constant of quartz; and $\hat{c}_v = c_v + \mathrm{j}\omega\eta_v$, where c_v is the elastic constant of the liquid and η_v is the liquid viscosity.

The electrical field within the quartz plate can be derived based on the constitutive equations of piezoelectricity as

$$\phi(y,t) = \left(\frac{e_{26}}{\in_{22}} A_1 \mathrm{e}^{\mathrm{j}k_q y} + \frac{e_{26}}{\in_{22}} B_1 \mathrm{e}^{-\mathrm{j}k_q y} + Cy + D\right)\mathrm{e}^{\mathrm{j}\omega t}. \tag{3}$$

The impedance of the sensor can be expressed as the ratio between the applied voltage and the current through the electrode as

$$Z = \frac{V}{I} = \frac{2\phi_0}{\mathrm{j}\omega \in_{22} \bar{A}} \frac{1}{C}, \tag{4}$$

where ϕ_0 is the electrical potential on the electrode and $\bar{A}$ is the effective area of the sensor.

There are six unknown constants A_1, B_1, A_2, B_2, C and D, in the harmonic solution, which should be determined from the boundary conditions as illustrated in figure 1. The boundary conditions include a stress free condition on the top surface overlayer; a stress free condition at the bottom of sensor; and the potential applied on the electrode surfaces. Another two boundary equations can be derived from the contact interface between the sensor surface and the bottom of the coating. The travelling thickness shear wave propagates into the liquid through the interface between the sensor and the coating. The interfacial condition does have a significant effect on the QCM response characteristics. Traditional treatment assumes continuous displacement and stress at the contact interface. The shear vibration energy of the sensor top surface is totally transferred to the liquid environment. The mass and the viscosity of the coating lead to a frequency reduction and flattening of the resonance of the impedance spectrum. However, recent research exhibited a significant deviation of the frequency shift between the measured results and evaluation results from continuous displacement and stress assumption. Interface slip can be a possible mechanism to explain this phenomenon [7, 8].

2.1. Spring–damper model of the contact interface

The interfacial slip between the quartz surface and the layer is modelled as a local molecular mass and an interaction element between the masses as shown in figure 1, as proposed in an early paper [14]. The interaction force between the two contacting molecular surfaces is modelled as the spring–dashpot force,

which is proportional to the relative displacement/velocity between the molecules of the two surfaces. The shear force at the interface is equal to the spring force plus the damping force. This assumption is valid when the relative deformation is small, which is within the linear elastic region. The lateral displacement of molecules in contact with the quartz surface is denoted u_q^h, and the displacement of a particle in contact with the liquid bottom is denoted as u_l^h. The equivalent shear force per surface unit of the interface can be expressed as

$$T_\mathrm{b} = G^*\gamma = \frac{G^*}{\delta}(u_q^h - u_l^h), \tag{5}$$

where δ is the distance between the molecules at the quartz surface and those in contact with the viscoelastic layer contact surface as shown in figure 1, $G^* = G' + \mathrm{j}\omega G''$ is the complex attraction parameter of the contact interfaces, G' being the spring stiffness, G'' the damper viscosity; γ is defined as $(u_q^h - u_l^h)/\delta$. The force maintaining the connection between the two contact surfaces is like the shear stress at the continuous medium. The single shear vibration mode is considered in the QCM compound resonator, and the particles at the surface have the same vibration phase. Based on the equations of motion for the particles in both the viscoelastic layer and the top of the quartz plate, another two boundary conditions on the interface between liquid and solid can be expressed as [14]

$$\begin{aligned}&\frac{G^*}{\delta}\mathrm{e}^{\mathrm{j}k_q h_1}A_1 + \frac{G^*}{\delta}\mathrm{e}^{-\mathrm{j}k_q h_1}B_1 \\ &\quad + \left[-\rho_l\Delta_l\omega^2 + \mathrm{j}\hat{c}_l k_v - \frac{G^*}{\delta}\right]\mathrm{e}^{\mathrm{j}k_v h_1}A_2 \\ &\quad + \left[-\rho_l\Delta_l\omega^2 - \mathrm{j}\hat{c}_l k_v - \frac{G^*}{\delta}\right]\mathrm{e}^{-\mathrm{j}k_v h_1}B_2 = 0, \end{aligned} \tag{6a}$$

$$\begin{aligned}&\left[-\rho_q\Delta_q\omega^2 + \mathrm{j}\hat{c}_q k_q + \frac{G^*}{\delta}\right]\mathrm{e}^{\mathrm{j}k_q h_1}A_1 \\ &\quad + \left[-\rho_q\Delta_q\omega^2 - \mathrm{j}\hat{c}_q k_q + \frac{G^*}{\delta}\right]\mathrm{e}^{-\mathrm{j}k_q h_1}B_1 + e_{26}C \\ &\quad = \frac{G^*}{\delta}\mathrm{e}^{\mathrm{j}k_v h_1}A_2 + \frac{G^*}{\delta}\mathrm{e}^{-\mathrm{j}k_v h_1}B_2, \end{aligned} \tag{6b}$$

where Δ_q and Δ_l are the particle thickness of the quartz contact layer and the liquid layer, respectively. The continuous displacement and shear assumption at the interface are replaced by a more detailed description of the contact interfacial properties.

2.2. Correlating with slip models presented

2.2.1. Explicit expression of the slip parameter. Ferrante *et al* [9] introduced an empirical description of the slip parameter, α, as the ratio between the complex displacement of the liquid bottom layer and the displacement of the sensor surface. The slip parameter was introduced to directly describe the motion of each compounded layer on the quartz crystal microbalance through a complex value, which can be expressed as

$$\alpha = \frac{u_v^h}{u_q^h} = \frac{A_2\mathrm{e}^{\mathrm{j}k_v h_1} + B_2\mathrm{e}^{-\mathrm{j}k_v h_1}}{A_1\mathrm{e}^{\mathrm{j}k_q h_1} + B_1\mathrm{e}^{-\mathrm{j}k_q h_1}}, \tag{7}$$

where u_v^h and u_q^h are the displacement of the liquid bottom layer and that of the sensor top surface, respectively. The slip parameter is a complex value, which includes the amplitude of the relative displacement and the phase angle between the two contact interfaces. Hayward and Thompson [7] used the slip boundary conditions in four-layer models of QCM, where the interface slip is included by the complex slip parameter, α, at each contact interface. Substituting the expressions for the constants A_1, A_2, B_1 and B_2, in equations (1) and (2), into equation (7), the slip parameter for QCM under a semi-infinite liquid can be expressed explicitly as

$$\alpha = \frac{G^*/\delta}{G^*/\delta + \rho_v\Delta_v\omega^2 + \mathrm{j}\hat{c}_v k_v}. \tag{8}$$

The distance between the atoms particles is of the order of 10^{-10} m. The part of the mass inertia of the contact particles, $\rho_v\Delta_v\omega^2$, is much smaller in comparison with the other two parts, G^*/δ and $\mathrm{j}\hat{c}_v k_v$, at operating frequencies of several megahertz.

2.2.2. Friction interface model. Rodahl and Kasemo [17] argued that the interfacial shear stress acting on the substrate is proportional to the relative velocity of the contact layers and can be expressed as

$$F_\mathrm{f} = \chi m_\mathrm{ML}(\dot{u}_q^h - \dot{u}_v^h), \tag{9}$$

where χ is the coefficient of friction between the contact interfaces and m_ML is the mass per unit area of the contact monolayer. McHale *et al* [10] employed the Stokes friction model in the circuit model to consider the interfacial slip of an acoustic wave device in a liquid. A single real parameter $s_1 = 1/\chi m_\mathrm{ML}$ is defined. Under the slip treatment, the acoustic impedance on the sensor surface induced by the overlayer is expressed as

$$Z_\mathrm{f}^\mathrm{s} = \frac{F_\mathrm{f}}{\dot{u}_q} = \frac{F_\mathrm{f}}{\dot{u}_v^h + sF_\mathrm{f}} = \frac{Z_\mathrm{f}}{1 + sZ_\mathrm{f}}, \tag{10}$$

where F_f is the force per surface unit exerted by the overlayer and $\dot{u}_q$ is the velocity of the monolayer on the sensor top surface; $Z_\mathrm{f} = F_\mathrm{f}/\dot{u}_v^h$ is the surface impedance for the non-slip model. Based on the spring–dash model, the shear stress exerted on the sensor surface can be expressed as

$$F_\mathrm{f}^\mathrm{s} = \frac{G'}{\delta}(u_q^h - u_v^h) + \frac{G''}{\delta}(\dot{u}_q^h - \dot{u}_v^h) = \left(-\mathrm{j}\frac{G'}{\omega\delta} + \frac{G''}{\delta}\right)(\dot{u}_q^h - \dot{u}_v^h). \tag{11}$$

The single parameter of the friction model is replaced by the complex value. The imaginary part of the attraction strength, G''/δ, corresponds to the real parameter, s, of the friction model employed by McHale *et al* [10]. Using Ferrante's results [9] for two TSM sensors with a hydrophilic coating and hydrophobic coating, the attraction strength calculated as a function of the liquid viscosity is illustrated in figures 2 and 3. It is found that the real part of the attraction strength, G', does have a more significant effect on the response than does the imaginary part of the attraction strength, G'' [14].

2.2.3. Contact slip length model. Ellis *et al* [11, 12] employed the slip length to replace the slip parameter, so as to provide a single parameter that can be linked to the physical quantities. The slip length, b, is defined as the distance from

the wall to the non-slip velocity as shown in figure 4 for fluid flowing at a stationary wall. For a quartz crystal microbalance with semi-unlimited liquid, the velocity, v_w, is the relative velocity between the top of the electrode surface and the bottom surface of the liquid, expressed as

$$v_w = \dot{v}_q - \dot{v}_v, \tag{12}$$

where $\dot{v}_q$ and $\dot{v}_v$ are the particle velocities of the contacted solid and liquid layers, respectively. Substituting equations (1) and (2) into equation (12), the relative velocity between two contact

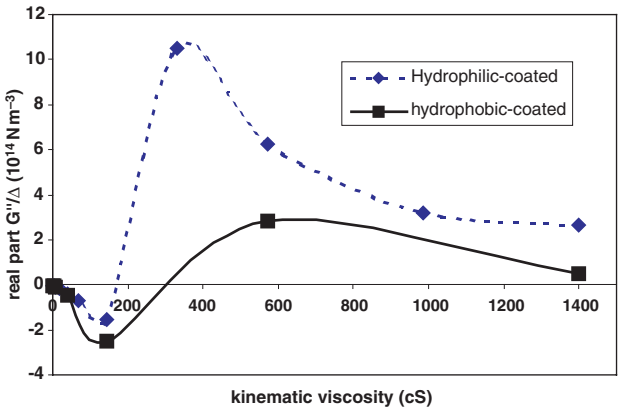

Figure 2. Real part of the interactive strength of the liquid–solid interface, G'/δ, as a function of the bulk liquid viscosity.

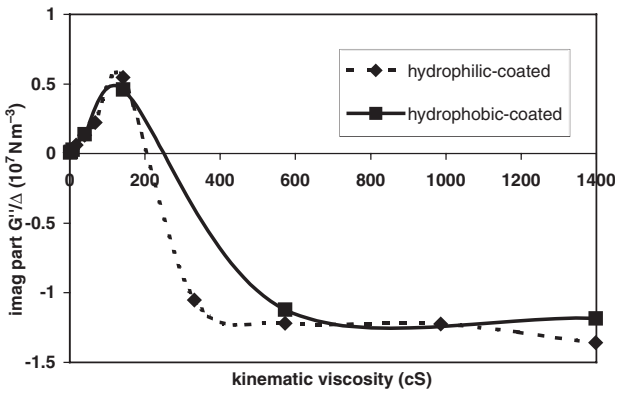

Figure 3. Imaginary part of the interactive strength of the interface, G''/δ, as a function of the bulk liquid viscosity.

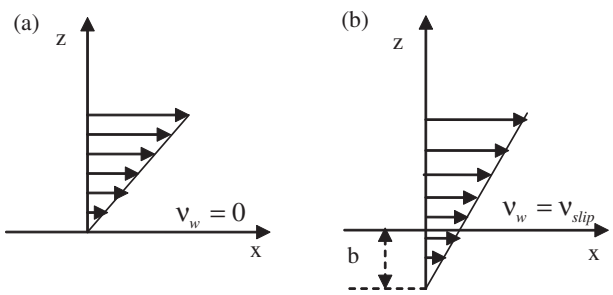

Figure 4. Velocity profile for (*a*) the non-slip condition $v_w = 0$ and (*b*) a slip condition with positive slip length b and wall velocity $v_w = v_{\text{slip}}$.

interfaces is expressed as

$$v_w = \mathrm{j}\omega(A_1\mathrm{e}^{\mathrm{j}k_q h_1} + B_1\mathrm{e}^{-\mathrm{j}k_q h_1} - A_2\mathrm{e}^{\mathrm{j}k_v h_1} - B_2\mathrm{e}^{-\mathrm{j}k_v h_1})\mathrm{e}^{\mathrm{j}\omega t}. \tag{13}$$

The slip length is used to stretch the velocity profile. For an oscillating wall, the velocity profile of the wall is moved out to match the surface velocity to be a continuous velocity profile as shown in figure 4:

$$v_q(h_1) = v_v(h_1 - b). \tag{14}$$

For a quartz crystal microbalance operating with a semi-infinite liquid loading, the constant $A_2 = 0$, so that the velocity boundary condition is rewritten as

$$A_1\mathrm{e}^{\mathrm{j}k_q h_1} + B_1\mathrm{e}^{-\mathrm{j}k_q h_1} = B_2\mathrm{e}^{-\mathrm{j}k_v h_1}\mathrm{e}^{-\mathrm{j}k_v b}. \tag{15}$$

Based on the mechanical slip interface model described in a previous section, one of the boundary conditions of the interface is expressed in equation (16). Similarly setting $A_2 = 0$, equation (5) can be rewritten as

$$\frac{G^*}{\delta}\mathrm{e}^{\mathrm{j}k_1 h_1}A_1 + \frac{G^*}{\delta}\mathrm{e}^{-\mathrm{j}k_1 h_1}B_1 = \left[\rho_v\Delta_v\omega^2 + \mathrm{j}\hat{c}_v k_v + \frac{G^*}{\delta}\right]\mathrm{e}^{-\mathrm{j}k_2 h_1}B_2. \tag{16}$$

Comparing equations (15) and (16), the relationship between the slip length and the attraction strength from the mechanical slip model can be expressed as

$$\cos(k_v b) + \mathrm{j}\sin(k_v b) = \frac{G^*/\delta}{\rho_v\Delta_v\omega^2 + \mathrm{j}\hat{c}_v k_v + G^*/\delta}, \tag{17}$$

where k_v is the wave number of the viscous liquid, which is related to the shear wave decay length in the liquid, χ, by

$$k_v = \sqrt{2\mathrm{j}}\sqrt{\frac{\omega\rho}{2\eta}} = \frac{\sqrt{2\mathrm{j}}}{\chi}. \tag{18}$$

Neglecting the mass inertia of liquid particles at the contact interface, the interfacial interaction strength can be expressed as

$$\frac{G^*}{\delta} = \frac{\sin(\sqrt{2\mathrm{j}}b/\chi) - \mathrm{j}\cos(\sqrt{2\mathrm{j}}b/\chi)}{1 - \cos(\sqrt{2\mathrm{j}}b/\chi) - \mathrm{j}\sin(\sqrt{2\mathrm{j}}b/\chi)}\frac{\hat{c}_v\sqrt{2\mathrm{j}}}{\chi}. \tag{19}$$

3. Fitting the experimental results

3.1. Experiment set-up

To investigate the slip of the interface between the liquid and the quartz surface, the resonance characteristics of the quartz crystal microbalance with bulk liquid loading, deionized water and ethanol were analysed experimentally. Quartz crystal microbalances operating at 5 MHz purchased from Stanford Research Systems (SRS) were used. The gold electrode pattern with what was called a 'wrap-around' configuration was used for proper operation in conductive liquids. The quartz crystal surface was optically clear, with about 50 Å average surface roughness. The QCM was clamped into the liquid flow cell (LFC). The LFC forms a chamber for the liquid with a volume approximately equal to 0.1 ml. Two pieces of

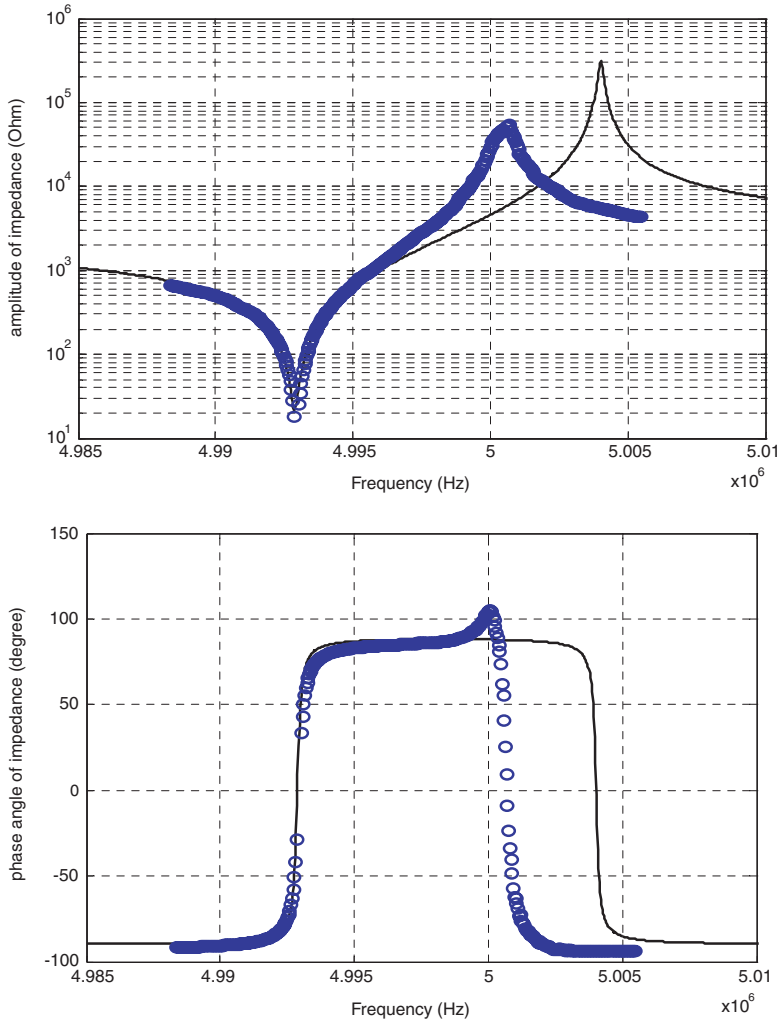

Figure 5. Measured amplitude and phase angle of the impedance response of a bare QCM and simulation results with fitting parameters (solid line—simulation results, lines of circles—experimental data).

quartz crystal microbalances from the same batch of samples were taken for surface modifications. The surface treatments involved (1) a 11-mercapto undecanoic acid (MUA) coating and (2) 1,6-hexanedithiol (HAT). The former would be more hydrophilic and the latter more hydrophobic. After the surface treatment, a self-assembled monolayer (SAM) was formed on the gold electrode surface. The QCM cells were washed with ethanol to remove loosely bound thiols and dried with nitrogen before measurement with the liquids.

A S&A 250B Network Analyser (Saunders & Associates, Inc., USA, with frequency range 1–100 MHz) was used, and the quartz crystal was connected through a standard 250B network analyser test head for impedance measurement. The impedance spectrum for dried bare QCM in LFC was used for fitting the simulation parameters. The oscillation system used was purchased from MAXTEK, which can record the series resonance frequency and resistance of resonance continuously.

Before assembled into the LFC, the QCM cell was washed with ethanol and deionized water, and dried using a nitrogen stream. After the dried bare crystal had been mounted in the LFC, the impedance spectrum of the system was measured using the S&A 250B Network Analyser for fitting the theoretical simulation parameters. Connecting the flow cell into the MAXTEK oscillating system, continuous measurements with deionized water and ethanol were taken without removing the crystal from the LFC. The same measuring sequences as for the QCM unmodified with deionized water and ethanol were taken for both the hydrophilic coated QCM and the hydrophobic coated QCM.

3.2. Parameter fitting for QCM in the air

The impedance spectra of three unperturbed QCMs in the unperturbed air condition were first recorded to fit the parameters of the theoretical simulation equation. The amplitude and the phase angle of the impedance spectrum of the bare QCM are illustrated in figure 5. The lines joining the circles represent the measured impedance amplitude and phase angle for the bare QCM under ambient conditions. The expression for the impedance of the QCM in air is [6]

$$Z = \frac{e_{26}^2}{\hat{c}_q k_q \epsilon_{22}^2 \omega \bar{A}} \tan\left(\frac{k_q h_1}{2}\right) - \mathrm{j}\frac{h_1}{\epsilon_{22} \bar{A} \omega}, \qquad (20)$$

Table 1. Experimentally measured series and parallel frequencies and the corresponding numerically fitted values for three QCMs in air.

	Experiment (MHz)		Numerical fitting (MHz)	
QCM in air	Series	Parallel	Series	Parallel
Bare QCM	4.992 89	5.000 31	4.992 89	5.004 02
HAT	4.994 26	5.001 79	4.994 26	5.005 41
MUA	5.006 82	5.014 45	5.006 82	5.017 96

Table 2. Parameters of the QCMs in air fitted for simulation from measured data.

QCM in air	Effective thickness, h_q (mm)	Effective contact area, $\bar{A}$ (m^2)	Viscosity, η_q ($N\,s\,m^{-2}$)
Bare QCM	0.331 572	$1.026\,49 \times 10^{-4}$	0.023 376
HAT	0.331 48	$1.163\,76 \times 10^{-4}$	0.024 376
MUA	0.330 65	$0.954\,88 \times 10^{-4}$	0.029 76

where the effective thickness of the QCM, h_q, the effective contact area, $\bar{A}$, and the effective quartz viscosity, η_q, are the parameters to be fitted from the experimental data. Other parameters of AT-cut quartz materials, the density $\rho_q = 2649\,kg\,m^{-3}$, crystal elastic shear modulus $c_{66}^q = 29.01 \times 10^9\,N\,m^{-2}$, the crystal dielectric constant $\epsilon_{33} = 39.82 \times 10^{-12}\,C\,V^{-1}\,m^{-1}$ and the piezoelectric constant $e_{26} = 0.0798\,C\,m^{-2}$ were taken from Hayward and Thompson [7]. It should be pointed that the effective thickness of the QCM is not the exact thickness of the quartz plate. There are metal layers formed on both the surfaces of the quartz plate. The series resonance frequency obtained for an uncoated crystal without metal and polymer by using the exact thickness of the quartz plate is higher than those measured with a metal layer coating. By adjusting the effective thickness of the QCM, the series resonance frequencies of the impedance spectrums measured are matched as shown in figure 5 with the solid line for the bare QCM. The parallel resonances are not well modelled since the electric effect of the metal layer and the connected leads is neglected, and the parallel resonant frequency decreased as the connected parallel capacity increased [7]. The measured and simulated resonance frequencies of three QCMs are listed in table 1, and the fitted effective parameters in air are listed in table 2.

3.3. Frequency shift with slip treatment

The series resonance frequency and the motional resistance were recorded as a continuous time-series data set. Figure 6 gives the frequency and resistance shift of the bare QCM with deionized water on top. The frequency and resistance changes were measured after the values had been stabilized. The ambient temperature was kept constant at 25°C. After removing the water from the chamber, the resistance and the frequency did not return back exactly to the original baseline as shown in figure 6. The frequency shift and the series resistance for the bare QCM and the monolayer coating QCMs are tabulated in table 3. Three types of surface combined with two different liquids give six pairs of different contact interfaces.

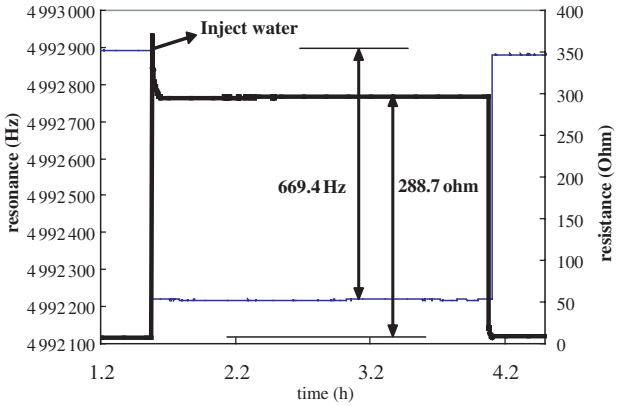

Figure 6. Frequency and resistance shift for the bare QCM in deionized water. Bold line—resistance; normal line—frequency.

For the devices in contact with it, the bare QCM produces the greatest frequency shift. The QCM with HAT surface modification gives a smaller frequency shift, because the hexanedithiol SAM for HAT QCM is hydrophobic and the deionized water is hydrophilic. The largest frequency shift of the bare QCM with water indicated that the bare QCM behaves more hydrophilic than the MUA QCM. When considering the interfacial slip between the solid and liquid, the series resonance frequency shift is a function of both the liquid viscosity, η_v, and the attraction strength, G^*/δ, which have been discussed with a theoretical simulation in an earlier paper [14]. The deviation between the non-slip assumption and the slip interface model is more significant when the devices are operated in a more viscous liquid.

When the viscosity of the bulk liquid is lower than a certain value, the low attraction strength between solid and liquid induces an even larger amount of frequency shift [14]. This can be explained by the fact that the viscosity of the water is quite low, about 0.914 cP. Thus, although the MUA QCM and water form strong bonds at the contact interface, the series resonance frequency shift can be smaller.

Figure 7 illustrates the impedance spectrum of the theoretical modelling of the bare QCM with bulk water loading. The parameters of the QCM are fitted from the experimental data as listed in table 4. In figure 7, the bold line is the impedance of the QCM in air fitted from measured results, the dotted line is evaluated from a continuous assumption and the solid line is evaluated from a mechanical slip model. The theoretical result for the frequency shift evaluated from the continuous interface assumption for bare QCM is 740 Hz, while the measured datum is only 669.4 Hz. There is an about 10% deviation between the theoretical result and the measured value. By adjusting the attraction strength of the contact interface between the solid and liquid, $G^*/\delta = (0.00824 + j0.0020) \times 10^{14}\,N\,m^{-3}$, in the mechanical slip model, a frequency shift of 680 Hz as shown in figure 7 can be obtained, which is closer to the measured value. Under the continuous interface assumption, the shear motion at the sensor surface is totally transferred to the liquid bottom layer. However, under the interfacial slip assumption, the vibration energy is partially transformed into the liquid, and the effect on the frequency shift of the QCM with the bulk liquid is smaller than that of the continuous assumption.

Table 3. Experimental data for series resonance frequencies for three types of QCM with semi-infinite liquids.

QCM	In air f_0 (Hz)	In water Δf_1 (Hz)	In water ΔR_1 (Ω)	In ethanol Δf_2 (Hz)	In ethanol ΔR_2 (Ω)
Bare QCM	4992 892.7	−669.4	288.7	−646	291.2
HAT QCM	4994 261.23	−579.72	273.5	−729.78	285.7
MUA QCM	5006 819.68	−652.85	292.9	−675.11	279.2

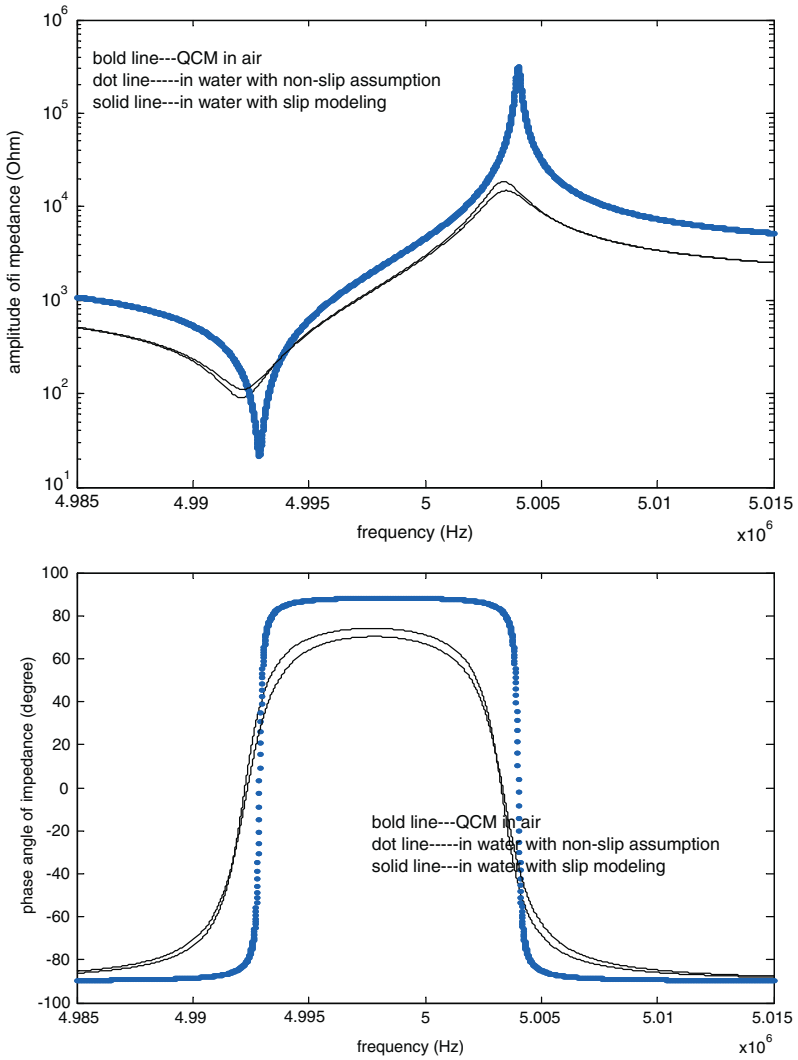

Figure 7. Theoretical evaluation of the impedance spectrum of the bare QCM with water loading on one surface with non-slip assumption and slip model ($G^* = 82.4 + 20\mathrm{j}\,\mathrm{N\,m^{-2}}$, $\delta = 10^{-10}$ m).

Table 4. Bulk liquid property parameters used in experiment for theoretical results.

	Density (kg m^{-3})	Viscosity (cP)	Stiffness (kPa)
Water	997.3	0.914	0.0
Ethanol	789.3	1.200	0.0

When the devices operate in ethanol, the trend of the frequency shifts for the three types of QCM is reverse in comparison with the trend when the liquid is water. The bare QCM presents the smallest amount frequency shift of 646.0 Hz and HAT QCM gives the largest frequency shift of 729.8 Hz. Based on the non-slip assumption, the frequency shift of the HAT QCM with ethanol on one surface is 752.2 Hz, which is larger than the measured results. With the assumption of a continuous displacement interface between the liquid and solid, the frequency shift can be evaluated by setting the contact attraction strength, G^*/δ, to be infinite. Comparing the experimental data and the theoretical frequencies for various liquids on the three QCM surfaces, there are large deviations between the experimental data and the theoretical values. Employing the mechanical slip interface model proposed as in the previous section, the frequency shift evaluated is normally smaller than that evaluated using the non-slip model.

Table 5. Frequency shift induced with semi-infinite liquid loading on one surface based on theoretical calculation (non-slip model and slip treatment).

	Bare QCM	HAT QCM	MUA QCM
Water			
Measured	−669.4 Hz	−579.7 Hz	−652.8 Hz
Non-slip	−740.1 Hz	−731.1 Hz	−741.7 Hz
Deviation	10.56%	26.12%	13.62%
Slip treating	−669.4 Hz	−579.7 Hz	−652.8 Hz
G^*/δ (10^{14} N m^{-3})	0.007 52 + j0.0020	0.005 229 + j0.0020	0.006 883 + j0.020
Ethanol			
Measured	−646.0 Hz	−729.8 Hz	−675.1 Hz
Non-slip	−755.2 Hz	−752.2 Hz	−756.9
Deviation	16.90%	3.1%	12.12%
Slip treating	−646.0 Hz	−729.8 Hz	−675.1
G^*/δ (10^{14} N m^{-3})	0.006 35 + j0.0020	0.011 84 + j0.0020	0.007 276 + j0.020

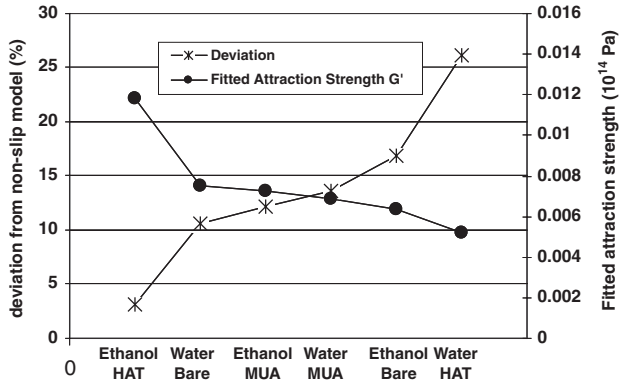

Figure 8. Frequency shift deviations from non-slip modelling and fitted attraction strength for TSM sensors in liquid.

By adjusting the attraction strength between the solid and liquid interface, the measured frequency shift can be matched. By using the least-squares iterative algorithm approach, the contact interaction strength between the solid and liquid, G^*/δ, can be determined. Table 5 lists the theoretical results of the frequency shift based on the non-slip model and slip model. The attraction strength is fitted based on the frequency shift. The imaginary part of the strength is set to be a constant value for comparison.

From the results in table 5, it is found that non-slip assumption gives a larger frequency shift compared with the real measured value when the QCM is operated in the lower viscosity liquid; and by adjusting the mechanical attraction strength based on the slip model, the measured value can be well matched. It is found that HAT QCM surface and ethanol present the highest interfacial interaction strength and the deviation from the non-slip assumption is lowest as shown in figure 8.

4. Conclusions and discussions

There are varied interpretations of the slip interface between the solid–liquid contact interfaces. The discontinuity of the interface induces the possibility of a shift of the frequency and Q-factor in the same direction. Theses models may have physically different descriptions. The coupling between the two contact interfaces is much more complicated. Under certain assumptions, the connection between the two contact layers can be described by a spring–dashpot system. The variable of the attraction strength is introduced in the electrical impedance of the QCM.

By surface modification, a monolayer with hydrodynamic properties coupling with the liquid was formed on the quartz crystal surface. The experimental investigation illustrated the deviation of the frequency shift between the measured results and the theoretical results from the continuous interface assumption. By adjusting the attraction strength of the contact interface in the slip modelling, the frequency shift of the experimental results can be matched. Comparing with the fitting results of the attraction strength, it is found that HAT QCM surface modification with HAT presents the largest attraction strength with ethanol and smallest attraction strength with water. This agrees with the fact that a HAT monolayer presents hydrophilic behaviour to water.

The solid–liquid interface characteristics present a much more complicated behaviour than with the continuous assumption. At the same time, there is currently no method of predicting the occurrence of interfacial slip and its strength at the acoustic wave device's surface. In this paper, it is attempted to present a framework to measure the interface attraction strength between solid and liquid contact layers by using a TSM resonator based on the mechanical slip interface model.

Acknowledgment

This work has been supported by Academic Research Fund, National University of Singapore under grant number R-265-000-151-112.

References

[1] Cernosek R W, Martin S J, Hillman A R and Bandey H L 1998 Comparison of lumped-element and transmission-line models for thickness-shear-mode quartz resonator sensors *IEEE Trans. Ultrason. Ferroelectr. Freq. Control* **45** 1399–407

[2] Tessier L, Schmitt N, Watier H, Brumas V and Patat F 1997 Poterntial of the thickness shear mode acoustic immunosensors for biological analysis *Anal. Chim. Acta* **347** 207–17

[3] Sauerbrey G 1959 Verwendung von schwingquarzen zur wagung dunner schechten and zur mikrowagung *Z. Phys.* **155** 206–22
[4] Nomura T and Okugara M 1982 Frequency shifts of piezoelectric quartz crystals immersed in organic liquids *Anal. Chim. Acta* **142** 281–4
[5] Reed C E, Kanazawa K K and Kaufman J H 1990 Physical description of a viscoelastically loaded AT-cut quartz resonator *J. Appl. Phys.* **68** 1993–2001
[6] Kanazawa K K 1997 Mechanical of films on the quartz microbalance *Faraday Discuss.* **107** 77–90
[7] Hayward G L and Thompson M 1998 A transverse shear model of a piezoelectric chemical sensor *J. Appl. Phys.* **83** 2194–201
[8] Tassew N and Thompson M 2002 RNA-peptide binding and the effect of inhibitor and RNA mutation studied by on-line acoustic wave sensor *Anal. Chem.* **74** 5313–20
[9] Ferrante F, Kipling A L and Thompson M 1994 Molecular slip at the solid–liquid interface of an acoustic-wave sensor *J. Appl. Phys.* **76** 3448–62
[10] McHale G, Lucklum R, Newton M I and Cowen J A 2000 Influence of viscoelasticity and interfacial slip on acoustic wave sensors *J. Appl. Phys.* **88** 7304–12
[11] Ellis J S and Hayward G L 2003 Interfacial slip on a transverse-shear mode acoustic wave device *J. Appl. Phys.* **94** 7856–67
[12] Ellis J S, McHale G, Hayward G L and Thompson M 2003 Contact angle-based predictive model for slip at the solid–liquid interface of a transverse-shear mode acoustic wave device *J. Appl. Phys.* **94** 6201–7
[13] Ellis J S and Thompson M 2004 Acoustic coupling at multiple interfaces and the liquid phase response of the thickness shear-mode acoustic wave sensor *Chem. Commun.* 1310–11
[14] Lu F, Lee H P and Lim S P 2003 Mechanical description of interfacial slips for quartz crystal microbalances with viscoelastic liquid loading *Smart Mater. Struct.* **12** 881–8
[15] Rosenbaum J F 1988 *Bulk Acoustic Wave Theory and Devices* (Boston, MA: Artech House) chapter 5
[16] Lu F, Lee H P and Lim S P 2004 Detecting solid–liquid interface properties with mechanical slip modeling for quartz crystal microbalance operating in liquid *J. Phys. D: Appl. Phys.* **37** 898–906
[17] Rodahl M and Kasemo B 1996 On the measurement of thin liquid overlayers with the quartz-crystal microbalance *Sensors Actuators* A **54** 448–56